



- Selective accumulation of dissolved organic matter in the
- sea surface microlayer: Insights from CDOM and
- 3 FDOM characterisation at a Mediterranean coastal site.

Elli Pitta, Eleni Tzempelikou, Christina Zeri

5 6

- 7 Institute of Oceanography, Hellenic Centre for Marine Research, 47 km Athinon Souniou ave., 19013
- 8 Anavyssos, Greece
- 9 Correspondence: Elli Pitta, ellip@hcmr.gr

10 11

12

13

14

15

16

17

18

19

20

21

22

23

24

25

26

27

28

29

30

31

32

33

34

35

36

37

38

Abstract

The sea surface microlayer (SML) is an extremely thin (~1 mm) boundary between the ocean and the atmosphere, forming a dynamic microenvironment that regulates air-sea gas exchange. Owing to its unique position, the SML is enriched with surface-active and hydrophobic organic compounds, typically more concentrated than in the underlying water (ULW), and can therefore modulate gas transfer across the interface. Despite its importance in ocean-atmosphere interactions, the processes governing its functioning remain insufficiently understood. This study investigates the biogeochemical coupling between the SML and ULW by examining the dynamics of dissolved organic matter (DOM)—including its chromophoric (CDOM) and fluorescent (FDOM) fractions—at a coastal Mediterranean site from 2016 to 2017. Twenty-two paired SML-ULW samples and fourteen rainwater samples were analyzed for dissolved organic carbon (DOC), UV-visible (250-700 nm) absorption spectra, and 3D fluorescence excitation emission matrices (EEMs). The SML was consistently enriched in DOC, CDOM, and FDOM relative to the ULW throughout the study. Enrichment factors (EFs) for long-wavelength absorption coefficients (a₃₀₀, a₃₇₀) exceeded 5. Relationships between a₃₀₀ and the spectral slope (S₂₇₅₋₂₉₅) indicated photodegradation in both layers, though more pronounced in the ULW. In the SML, photodegradation effects appeared to be partially counterbalanced by in situ production or aggregation of hydrophobic, optically active, higher-molecular-weight material. Parallel Factor Analysis (PARAFAC) identified four FDOM components: two humic-like (A/C, A/M) and two protein-like (T, B). Terrestrial humic-like (A/C) and tryptophan-like (T) fluorophores were dominant and strongly enriched in the SML (EF > 4). By introducing an FDOM/CDOM index, a decoupling between fluorescent and non-fluorescent chromophoric organic fractions was revealed: the SML exhibited higher fluorescence in the UV-C/UV-B regions (A, B, T peaks) but lower fluorescence in the UV-A/visible region (C peak), suggesting selective accumulation of absorbing but non-fluorescent CDOM. Potential drivers of this decoupling include biological transformations, rapid microlayer reorganization, and atmospheric inputs. Rainwater showed DOC concentrations and absorption features comparable to the SML but distinct fluorescence characteristics. PARAFAC modeling of rainwater did not resolve the tryptophan-like fluorophore and revealed blue-shifted humic-like components, consistent with photochemically aged, low molecular weight DOM of mixed marine-terrestrial origin. Overall, the results indicate that photodegradation,







biological activity, rapid molecular reorganization, and atmospheric deposition collectively shape the
 wavelength-dependent enrichment of CDOM and FDOM in the SML, highlighting its active role in air—
 sea biogeochemical exchange.

42

1. Introduction

43 44 45

46

47

48

49

50

51

52

53

54

55

56

57

58

59

60

61

62

63

64

65

66

67

68

69

70

71

72

73

74

75

76

77

The sea surface microlayer (SML) represents the boundary interface between the ocean and the atmosphere. Having a thickness of less than 1 mm, it ubiquitously covers the ocean surface. The formation and persistence of the SML are generally considered to be strongly influenced by wind speed (Liss & Duce, 1997). However, recent findings suggest that the relationship between SML stability and wind conditions is not straightforward, as enrichment can occur even under high wind speeds (Sabbaghzadeh et al., 2017; 2024). Beyond wind effects, other factors—including solar radiation, which drives photochemical and microbial processes; biological activity, which produces and modifies surfaceactive substances; and atmospheric deposition—play critical roles in determining the composition and persistence of the SML (Wurl & Holmes, 2008; Cunliffe et al., 2013; Upstill-Goddard, 2006). These physical, chemical, and biological interactions collectively define the dynamic nature of the SML and its influence on air-sea exchange processes. Enriched with surfactants, the SML can significantly impede the air-sea transfer of greenhouse gases such as CO₂, CH₄, and N₂O by acting as a physical barrier (Liss & Duce, 1997; Pereira et al., 2018). Studies suggest that the presence of the SML can reduce CO₂ fluxes by 15-50%. However, most gas exchange models neglect this effect, leading to potential errors of up to 20% in regions with elevated surfactant concentrations (Asher, 1997; Mustaffa et al., 2020). Integrating SML dynamics into climate models is therefore essential for refining global gas flux estimates and improving our understanding of ocean-atmosphere interactions (Milinković et al., 2022). The sea surface microlayer (SML) is characterized by a high content of hydrophobic, surface-active compounds such as carbohydrates, proteins, lipids, and humic substances, as well as particulate organic matter and a diverse community of autotrophic and heterotrophic microorganisms (Hunter, 1981; Cunliffe et al., 2009; Cunliffe et al., 2013). The enrichment of dissolved organic matter (DOM) in the SML is a complex process (Mustaffa et al., 2018), primarily driven by the continuous supply of organic material from the underlying seawater through biological activity and selective scavenging mechanisms (Liss & Duce, 2005; Obernosterer et al., 2008; Penezić et al., 2022). Additional sources of organic matter include terrestrial and atmospheric inputs, as well as in situ production and release by primary producers and bacteria (Hardy, 1982; Wurl & Obbard, 2005; Wurl et al., 2009; Stolle et al., 2010; Ebling & Landing, 2017). The SML often exhibits spatial heterogeneity due to the accumulation of floating particulate material at the surface (Hunter, 1980), resulting in patchy distributions or slicks enriched in surfactants and potentially characterized by elevated biological productivity (Ploug, 2008; Ribas-Ribas et al., 2017). Chromophoric dissolved organic matter (CDOM) represents the fraction of DOM capable of absorbing light in the ultraviolet (UV) and visible regions. A subset of CDOM, known as fluorescent dissolved organic matter (FDOM), can additionally emit light upon excitation in these spectral ranges. In marine environments, CDOM is produced in situ through processes such as primary production, bacterial





78 activity, cell metabolism and lysis, and the leakage of material from particulate organic matter. External 79 inputs also contribute to CDOM levels, including terrestrial sources delivered via riverine and land 80 runoff, sewage discharges, and atmospheric deposition through precipitation. The primary removal 81 mechanisms of CDOM in surface waters are photodegradation driven by UV radiation and bacterial 82 mineralization. Over the past decades, CDOM has received considerable attention due to its key role in 83 carbon cycling, the bioavailability of trace elements, and the air-sea exchange of trace gases (Mopper et 84 al., 1991; Zepp, 1998; Coble, 2007). Moreover, CDOM strongly influences light attenuation in the ocean 85 (Kirk, 1994; Siegel & Michaels, 1996; Nelson et al., 1998), thereby affecting primary productivity. 86 Consequently, the optical properties of CDOM at the ocean surface have significant implications for 87 remote sensing applications, particularly in relation to chlorophyll-a retrievals and ocean colour 88 observations (Tassan, 1988; Hoge et al., 1995). 89 Enrichment of CDOM in the SML relative to the underlying water (ULW) has been reported in several 90 studies (Obernosterer et al., 2008; Mustaffa et al., 2017, 2018). CDOM consists of large, complex 91 molecules rich in unsaturated bonds and aromatic moieties, structural features that impart hydrophobic 92 properties favouring its accumulation within the SML. In coastal regions, terrestrial inputs can contribute 93 substantially to the CDOM pool, while intense photochemical processes at the sea surface can 94 significantly modify its composition. Interaction with sunlight can lead to CDOM mineralization and 95 removal, accompanied by CO2 and CO emissions, or to the breakdown and formation of less complex 96 organic compounds that are more susceptible to bacterial transformation and degradation (Gao & Zepp, 1998; Moran et al., 2000; Zhang et al., 2013; Logozzo et al., 2021). Spatially, CDOM distribution within 97 98 the SML is often patchy, with elevated concentrations occurring in slicks and other surface accumulations 99 (Wurl et al., 2009; Mustaffa et al., 2017). Despite its ecological and biogeochemical importance, CDOM 100 dynamics in the SML remain insufficiently explored, particularly under the distinct physical and 101 chemical conditions characteristic of this boundary layer. 102 The present study investigates the nature, sources, and transformation processes of CDOM/FDOM in the 103 SML compared to the ULW in a Mediterranean coastal site, using high-resolution temporal data obtained 104 from biweekly sampling over a one-year period. In addition, we examine rainwater CDOM/FDOM in 105 order to investigate potential linkages between the optical signatures of rainwater and those observed in 106 the SML. We anticipate that the results will provide new insights regarding CDOM dynamics in the 107 SML.

108

2. Materials and Methods

109110

2.1. Study area and sampling strategy

111112113

114

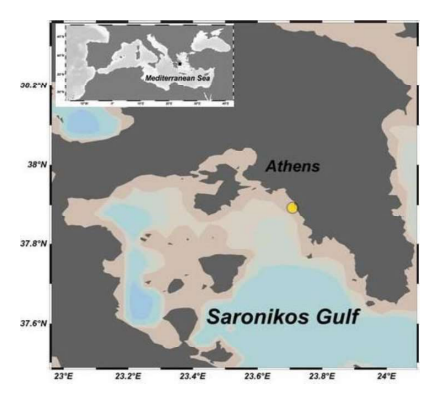
115

116

The sampling site is located in the south-east Saronikos Gulf about 1km from the coast in the eastern Mediterranean (Fig. 1). Due to its proximity to the coast the site is affected by urban runoff while only a small urban stream outflows in the area. Two phytoplanktonic blooms in the spring-early summer and autumn-early winter are characteristic for the area (Kitsiou and Karydis, 2000; Zervoudaki et al., 2022).







118119

120

121

122

123

124

125

126

127

128

129

130

131

132

133

134

135

136

137

138

139

140

141

142

143

144

Figure 1: Study area, the yellow dot marks the sampling site in the Saronikos Gulf

The study covered an annual cycle from June 2016 to June 2017. During this period data for wet

precipitation (mm), solar radiation from the National Observatory of Athens (www.meteo.gr) and dust episodes and deposition (μg m⁻³) from Skiron Forecasting system (https://forecast.uoa.gr/en/forecast-maps/skiron) have been gathered. Saharan dust events were also confirmed via the EOSDIS Worldview (https://worldview.earthdata.nasa.gov/) (Table S1). Seawater samplings were performed almost twice per month under low wind speed conditions (< 4 ms⁻ 1). Seawater temperature (T) and salinity (S) were recorded in situ using a CTD (Seabird electronics, Bellevue, WA, USA) instrument. Wind speed was recorded with a portable anemometer Benetech GM816. Samples were collected from SML and from 1m depth representing the UWL, in total 22 pairs. SML was sampled following the glass plate technique (Harvey and Burzell, 1972) yielding a microlayer thickness of $50 \pm 10 \mu m$ (Zhang et al., 2003) (Table S). A 30 x 30 cm glass plate sampler with a width of 4 mm was used. Samples from the ULW were collected using a Niskin sampling bottle. Samples for DOC and CDOM/FDOM analysis were collected in amber glass containers with teflon caps while samples for chl-a determination in HDPE containers; refrigerated and immediately transported to the laboratory, where they were filtered through 0.22 µm polycarbonate filters previously rinsed with Milli-Q water. Filtered samples for DOC analysis were kept in precombusted (450°C, 12h) glass ampoules, acidified with HCl 2N at pH~2, sealed and stored at ~4°C until analysis. Filtered samples for absorption and fluorescence analysis were kept in amber glass bottles with teflon cups and stored at ~4°C until analysis. The glass containers used during sampling and for the storage of CDOM/FDOM samples were previously acid cleaned (HCl 10%, 12h) and rinsed thoroughly with Milli-Q water. Filters for chl-a determination were preserved frozen (-20°C) in the dark until analysis. For the period December 2016 to May 2017 rainwater samples were collected (14 samplings), via a simple system made with a Nalgene bottle connected to a HDPE funnel for wet deposition (Azimi et al.,

2003) situated on the roof of a building at the coast of the study site. This was an open system, so it is

assumed it was affected by dry deposition passively collected when not raining. Details on the study site

and sampling procedure are described in Tzempelikou et al., (2025).





2.2. Chlorophyll-a (Chl-a)

Chl-a was determined according to the Holm-Hansen et al., (1965) method using fluorescence detection in a TURNER fluorometer model TD 700. An initial sample volume equal to 500mL was filtered for

151 SML and 1.5L for ULW.

2.3. Dissolved Organic Carbon (DOC) analysis

The determination of DOC (mg L⁻¹) in the samples was performed using a Shimadzu TOC-L organic carbon analyzer following the High Temperature Catalytic Oxidation, HTCO. The system was standardized prior analysis using a potassium hydrogen phthalate standard solution series. Each sample was injected 3 to 5 times and DOC concentration was estimated as the average value of three replicates that yielded standard deviation <2%. Analytical precision and accuracy were tested daily prior and at the end of the analysis using Deep Atlantic Seawater Reference Material provided by the DOC-CRM program (University of Miami - D.A. Hansell). The certified value of the reference material is 0.480-0.528 mg L⁻¹ (Batch 19 Lot 10-19) and the measured values (n=22) during the analysis of the samples were between 0.478 - 0.530 mg L⁻¹ indicating that no drift correction was necessary.

2.4. Absorption analysis

Samples for absorption determination were allowed to reach room temperature before analysis. Absorption spectra were obtained between 250 and 700nm at 1nm increments using a dual beam UV-visible spectrophotometer (Perkin Elmer, Lambda 25) equipped with 5cm quartz cells and referenced to Milli-Q water. A blank scan (Milli-Q) was measured frequently to assure the stability of the instrument and it was also subtracted from each sample spectra for baseline correction. Absorption units were converted to absorption coefficients through the relationship:

 $a(\lambda) = 2.303 * A(\lambda)/1$

where $a(\lambda)$ is the absorption coefficient (m^{-l}) at wavelength λ , $A(\lambda)$ is the absorbance at the certain wavelength and l is the light path length in meters.

wavelength and l is the light path length in meters.

Absorption coefficient at 300nm wavelength was used for the representation of bulk CDOM. However, 3 more wavelengths (265 nm, 280 nm, 370 nm) were used in order to investigate whether there are differences in CDOM profiles in the different regions of the spectrum between the SML and ULW. The wavelengths selected provide a good coverage of the spectrum and correspond to wavelengths of maximum fluorescence intensities of the samples (see section 2.5). Wavelength 265nm falls in the UV-C region, wavelength 280nm is the border between UV-C and UV-B region, wavelength 300nm belongs to the UV-B region while wavelength 370nm falls in the UV-A region and it is also close to the visible light preserving though high absorption values. No wavelength of the visible region (>400nm) was chosen due to the low absorption values especially in the ULW.

Spectral slope of the narrow region 275-275, S₂₇₅₋₂₉₅ (nm⁻¹) of the spectra was calculated using linear

regression of the log-transformed spectra. This is a useful indicator of the molecular weight and source





composition of CDOM and can be determined with high precision, even in highly photobleached openocean environments (Helms et al., 2008). Consequently, it is often favored over other spectral slope indices. Photodegradation processes typically lead to a reduction in DOM molecular weight, resulting in elevated $S_{275-295}$ slope values, whereas microbial transformation generally decreases this spectral slope through the production of higher-molecular-weight organic compounds that exhibit strong absorption within the 275-295 nm range. (Helms at al., 2008; Fichot and Benner, 2009; Ortega-Retuerta et al., 2009)

192193194

187

188

189

190

191

2.5. Fluorescence Analysis

195196

197

198

199

200

201

202

203

204

205

206

207

208

209

210

211

212

213

214

215

216

217

218

219

220

221

222

223

224

225

226

Fluorescence was measured using a Horiba Aqualog-UV-800 spectrofluorometer equipped with a 150W ozone-free xenon arc-lamp and a 1cm quartz cell. Excitation- Emission Matrices (EEMs) were obtained between 240 and 450nm (5nm increments) for excitation and between 250 and 800nm (~0.6nm increments) for emission. The integration time of the measurement was adjusted according to the fluorescence intensity in the SML and ULW samples. A blank EEM (Milli-Q water) was measured daily and subtracted from each sample in order to correct Raman and Rayleigh scattering. All EEMs were corrected for inner filter effect following the Aqualog Operations Manual and were normalized to Raman Units (R.U.) using the Raman scatter emission peak of Milli-Q (Lawaetz and Stedmon, 2009) obtained after the measurement of each sample. The collected EEMs were further analyzed using Parallel Factor Analysis (PARAFAC). PARAFAC was performed following Murphy et al. (2013) using MATLAB R2015a and the "drEEM toolbox". Prior modeling, the emission region between 550 and 800nm was removed since no significant CDOM fluorescence signal was detected. The subtraction of Milli-Q water from the EEMs did not remove sufficiently the Rayleigh and Raman scatter peaks and thus both first and second order Rayleigh and Raman scatter bands were interpolated using the "smootheem" function of the drEEM package. All EEMs were then normalized to their total signal to tackle the large concentration gradients that were observed between the SML and ULW. The model was run five times with random initial values and model validation was carried out through split half analysis using four splits yielding six different combinations and it was repeated five times (S₄C₆T₅). The convergence criterion was 10⁻⁶. Visual inspection of the residuals was also implemented along with split half analysis to assure randomness (Pitta and Zeri, 2021). PARAFAC analysis was performed on the seawater EEMs (SML-ULW, n=22). An additional PARAFAC model was conducted for the rainwater EEMs (n=14). Spectral characteristics of the components resolved by the seawater and rain water models are given in Table S2. For the calculation of the FDOM/CDOM index discussed in Section 4.3 we extracted the numeric values of modelled intensities of the scattering corrected EEMs derived from the 'smootheem' function of the DrEEM package. The fluorescence intensity (I_{ij}) at each excitation wavelength (Ex_i) was then divided by the corresponding absorption coefficient (ai) obtained from the absorption measurements. This was repeated for all emission wavelengths (Em_i), thus yielding the ratio I_{ij}/a_i i.e. the FDOM/CDOM (R.U.m) index, in the form of a 3-dimensional matrix where Ex=250-450nm and Em=260-550nm (Suppl Fig. S1). We then calculated the average FDOM/CDOM index for all the samples in the SML and ULW separately. First step was the construction of 291 (number of emission wavelengths) n × 41 matrices





227 (where n is the number of samples in each dataset and 41 is the number of excitation wavelengths) using 228 the FDOM/CDOM matrices of the samples in each layer. Next, we calculated the average of each column of the 291 (n × 41) matrices resulting into 291 1 × 41 vectors. Finally, 291 1 × 41 vectors i.e. the average 229 230 FDOM/CDOM were illustrated in a 3-dimensional plot. This analysis was performed in MATLAB 231 R2015a using in-house functions. 232 233 2.6. Enrichment factor (EF) 234 235 The Enrichment Factor, EF, of the various measured parameters in the SML is calculated as the ratio of 236 the measured values in the SML to the measured values in the ULW: 237 $EF = C_{SML}/C_{ULW}$ 238 where C_{SML} is the concentration of any parameter in the SML and C_{ULW} its corresponding concentration 239 in the ULW. EF values ≥ 1 indicate enrichment in the SML, while EF values ≤ 1 indicate depletion. 240 241 2.7. Statistical analysis 242 243 The variability of the measured parameters between SML and ULW was evaluated using the Mann-244 Whitney U test, as the data did not meet the assumptions required for parametric analysis. For the same 245 reason, deviations of enrichment factors from unity were assessed using the one-sample Wilcoxon 246 signed-rank test. Linear regression and Spearman correlation was applied to evaluate relationships 247 among the measured parameters. All reported regression and correlation coefficients (R2 and r 248 respectively) are statistically significant (p < 0.05). All analyses were conducted using IBM SPSS 249 Statistics, Version 20.0. 250 251 3. Results and discussion 252 253 3.1. Environmental and physicochemical conditions 254 255 Figure 2(a) presents the timing and intensity of rain and dust events recorded between 2016 and 2017, illustrating that the study site was influenced by both wet and dry atmospheric deposition. Over the 376-256 257 day observation period, Saharan dust was detected on 103 days (27%), comprising 77 dry dust pulses 258 and 26 dusty rain events, while dust-free rainfall occurred on 31 days (8%). Solar irradiance exhibited pronounced seasonality, peaking in summer-autumn (600-900 W m⁻²) and reaching minima during 259 260 winter (130-500 W m⁻²). Seawater temperature (T) varied between 17 and 26 °C from June 2016 to 261 January 2017, dropped to ~14 °C in February-March 2017, and increased again by May. Salinity 262 remained relatively stable (38.06–39.61 psu) throughout the study period (Table S1). 263 Chl-a concentrations in the SML and ULW are shown in Fig. 2(b). Values ranged from 0.21 to 0.88 µg

 L^{-1} (average = 0.51 $\mu g \ L^{-1}$) in the SML and from 0.13 to 0.83 $\mu g \ L^{-1}$ (average = 0.44 $\mu g \ L^{-1}$) in the ULW,

consistent with the region's meso-oligotrophic character. No significant difference was detected between





layers (p > 0.05), and SML enrichment was minimal (EF = 1.2 ± 0.3). The annual Chl-a distribution revealed an unexpected summer peak in July 2016 followed by a secondary maximum in autumn, indicative of an autumn bloom. Thereafter, concentrations declined in winter and increased again in early spring. It should be noted that Chl-a was determined using a finer filter (0.22 μ m instead of the standard ~0.8 μ m GF/F), likely capturing smaller phytoplankton cells and yielding marginally higher values (Tzempelikou et al., 2025). Moreover, the occurrence of multiple Saharan dust pulses during our study period is expected to enhance primary production, consistent with observations in the Mediterranean ecosystem (Astrahan et al., 2016; Gallisai et al. 2014).

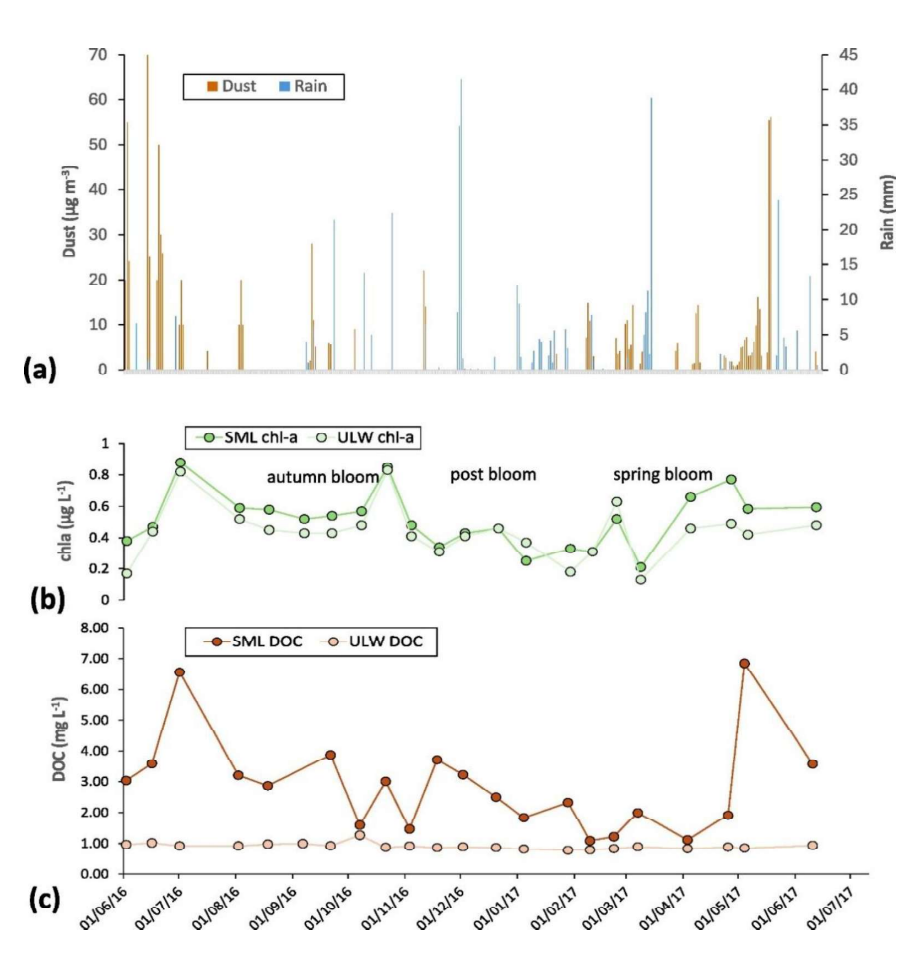


Figure 2: Monthly variation of (a) Saharan dust ($\mu g \ m^{-3}$) and rain (mm) deposition, (b) chl-a ($\mu g \ L^{-1}$) and (c) DOC (mg L^{-1}) during the sampling period. (a) Dust is given in orange and rain in blue (b,c) dark dots correspond to SML concentrations and light colored to ULW ones.

The environmental conditions during our study period (low wind speed, relatively elevated dust particles and chl-a) favored pronounced SML formation, as evidenced macroscopically by apparent surface slicks in 12 of the 22 samplings (Table S1). These gel-like surface slicks are formed primarily by surfactants,





are rich in hydrophobic organic matter and can host microorganisms and particles forming a distinct ecosystem in the SML compared to the ULW (Zancker et al., 2017; Wurl et al., 2016). Indeed, accumulation of phytoplankton exudates such as gel-like transparent exopolymer particles (TEPs) has been recorded for the area during the same period (Tzempelikou et al., 2025).

3.2. Dissolved organic carbon in the SML and UWL

Annual variability of DOC concentrations in the SML and ULW is shown in Fig. 2(c). In the SML, DOC ranged from 1.09 to 8.33 mg L⁻¹, with an average concentration of 3.13 mg L⁻¹, significantly higher than that in the ULW (average: 0.93 mg L⁻¹; range: 0.78–1.23 mg L⁻¹; p = 0.001). Two exceptionally high DOC values observed in the SML (01 July 2016 and 04 May 2017) were not reflected in the ULW, suggesting episodic enrichment events. DOC dynamics in the SML tracked those in the ULW during winter but diverged substantially during summer and autumn (Table S1). Consequently, DOC concentrations between the two layers were weakly but significantly correlated (r = 0.463; p = 0.046, excluding the two extreme values) indicating that apart from upward transport of DOM other processes affect the DOC pool in the SML.

Significant correlation of several DOM compounds between the SML and ULW is a common feature across studies indicating that upward transport of material plays a dominant role in the composition of the SML in DOM (Chen et al., 2013; 2016; Engel and Galgani, 2016). Furthermore, the DOC enrichment factor (EF = 2.7 ± 1 ; p = 0.001; Fig. 3(a)) confirms substantial accumulation of DOM components in the SML.

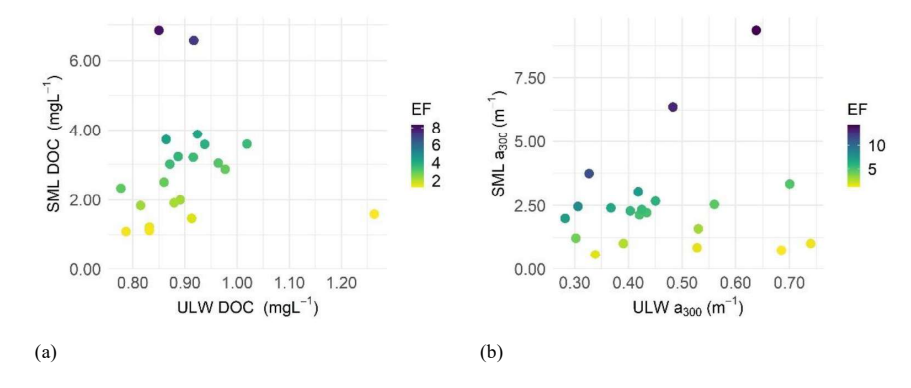


Figure 3: Correlation graphs between the SML (y axis) and ULW (x axis) of (a) DOC (mg L^{-1}); (b) absorption coefficient a_{300} (m $^{-1}$). The z axis illustrates the enrichment factors

3.3. CDOM dynamics within the DOM pool in SML and ULW

The distribution of the absorption coefficients at 300nm, $a_{300}(m^{-1})$ in the SML and ULW is presented in Fig. 3 (b), (see Table S3 for wavelengths 265, 280, 370 nm). In the SML, a_{300} ranged from 0.569 to 9.347

308

309

310

311

312

313

314

315

316317

318

319

320

321

322

323

324

325

326

327

328

329





m⁻¹, with an average of 2.565 m⁻¹. The distribution of a₃₀₀ (m⁻¹) closely mirrored the one of DOC, displaying maxima on 01 July 2016 and 04 May 2017. As observed in the case of DOC, a₃₀₀ values in the ULW were significantly lower (p = 0.001), and the high SML peaks were not reflected in the ULW. The lack of correlation between a₃₀₀ in the two layers (Fig. 3(b)) suggests that CDOM originates from different sources and undergoes distinct processes rather than being influenced primarily by upward flux, highlighting the additional roles of in situ photochemical or biological transformations and/or direct atmospheric inputs to the optically active DOM pool. In the SML, DOC was strongly correlated with a₃₀₀ indicating that the variations in CDOM are largely driven (by 77%) by those in the bulk DOM. In contrast, no significant correlation between DOC and CDOM was observed in the ULW (Table 1). The overall strong coupling between the optically active fraction of DOM and bulk DOM in the SML suggests shared sources and transformation dynamics, whereas their decoupling in the ULW implies that DOM and CDOM respond differently to biogeochemical and photochemical processes taking place in the ULW. Enrichment factors (EFs) of $a(\lambda)$ were consistently and significantly greater than unity (p < 0.05), confirming systematic enrichment of CDOM in the SML as observed in previous works (Obernosterer et al., 2008; Wurl et al., 2009; Lechtenfeld et al., 2014; Mustaffa et al., 2017). Moreover, EFs increased progressively from the UV-C (a₂₆₅) (EF=3.6) to the UV-A/near-visible regions (a₃₇₀) (EF=7.4) (Table S4), indicating wavelength-dependent accumulation of chromophoric material at the surface. Yang et al., 2022 also reported higher EFs in longer wavelengths in the eastern marginal seas of China. UV-A/nearvisible chromophores are disproportionately enriched at the surface, highlighting a decoupling of CDOM constituents in the SML relative to the underlying water.

Table 1. Linear regression analysis of DOC *vs* absorption coefficients in SML, ULW and rain waters (excluding the outlier values of 01 July 206 and 04 May 2017).

| | equation | R^2 | p |
|--------------|----------------|-------|-------|
| SML (n=22) | | | |
| DOC vs a300 | y=0.844x-0.094 | 0.774 | 0 |
| ULW (n=22) | | | |
| DOC vs a300 | - | 0.073 | 0.224 |
| Rain (n= 14) | | | |
| DOC vs a300 | y=1.225x+0.534 | 0.878 | 0 |

330 331

332

333

334

335

336

337

338

Spectral slope values $S_{275\cdot295}$ in the SML ranged from 0.015 to 0.034 nm⁻¹ with an average of 0.025 nm⁻¹. In the ULW $S_{275\cdot295}$ values were considerably (p=0.001) higher than those in the SML fluctuating between 0.029-0.039 nm⁻¹ with an average of 0.034 nm⁻¹. The increase in spectral slope $S_{275\cdot295}$ (nm⁻¹) i.e. a steeper absorption spectra, usually reflects a decrease in molecular weight, and when plotted against the absorption coefficients a_{300} (m⁻¹), typically exhibits a negative trend (Chin et al., 1994; Weishaar et al., 2003; Helms et al., 2008; Tzortziou et al., 2011). This relationship is commonly used to interpret changes in CDOM resulting from photodegradation processes in surface waters (Helms et al., 2008; Fichot and Benner, 2012). The relationship tends to be linear within a compositionally uniform DOM

340

341342

343

344

345

346

347

348

349 350

351

352

353

354

355

356





source (Helms et al., 2008; Twardowski and Donaghay, 2001) while it becomes nonlinear (often exponential) across natural gradients encompassing a wide range of CDOM concentrations or mixed sources (e.g., riverine and marine), due to the coexistence of DOM with differing molecular compositions and reactivities (Fichot and Benner, 2012; Nelson and Siegel, 2013). In Fig. 4, this relationship is presented against a₃₀₀ (m⁻¹). It is evident that for the ULW, the relationship between the two parameters exhibits a steeper slope compared to the SML. Furthermore, for both layers combined, the a_{300} vs $S_{275-295}$ relationship is well described by an exponential decay equation R²=0.791 (y=0.020*e-1.572*x+0.023) indicating different CDOM composition in the two layers. These observations indicate photodegradation of CDOM in both the SML and ULW. Yet, the less steep/moderate slopes found for the a_{300} vs $S_{275-295}$ relationship in the SML suggest that other processes taking place in the SML probably compensate the effect of photodegradation. Possible explanations are the continuous reorganization of the hydrophobic DOM in the SML, (Wurl et al., 2009; Lechtenfeld et al., 2014; Mustaffa et al., 2017, Penezic et al., 2022) and/or the in-situ production of optically active material in the UV-A -near visible region in the SML. Galgani and Engel (2016) have observed a decrease in spectral slope in the SML due to the abundance of bacterial and phytoplankton cells in parallel to elevated gelatinous material (Coomassie particles and TEPs), thus corroborating to SML specific processes leading to the production of higher molecular weight CDOM.

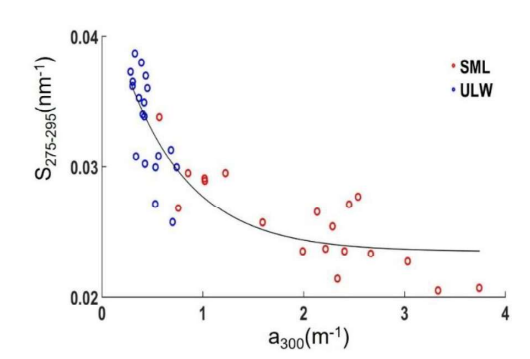


Figure 4: Relationship between $a_{300}(m^{-1})$ and $S_{275-295}(nm^{-1})$ in the SML (red circles) and ULW (blue circles). When both layers are combined the relationship is well approximated by an exponential decay equation denoting multiple chemical structures of CDOM compounds

As previously noted, absorption was noticeably higher in the SML on 01 July 2016 and 04 May 2017, following the trends observed in DOC concentrations. Alongside these elevated absorption values, the SML spectra exhibited two distinct shoulders at approximately 330 nm and 360 nm, features that were absent in the respective spectra in the ULW (Fig. 5).

361

357

358





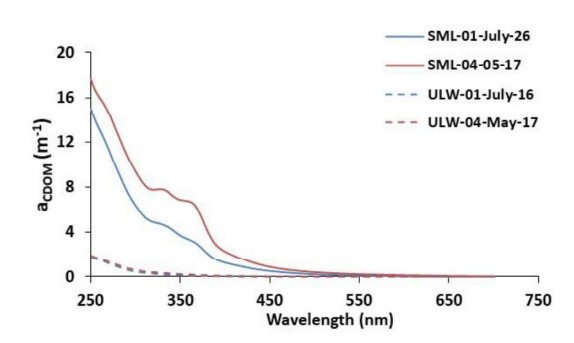


Figure 5: Absorption spectra in the SML (solid lines) and ULW (dashed lines) on 01 July 2016 (blue) and 04 May 2017 (red). Spectra shoulders at 330 nm, 360 nm are indicative of MAA absorption

Tilstone et al. (2010) reported pronounced UV absorption shoulders at 300–340 nm, coinciding with elevated concentrations of mycosporine-like amino acids (MAAs), particularly during surface slicks. These high MAAs levels were linked to coastal phytoplankton blooms and associated exudation, which protect cells from solar irradiance and tend to accumulate in the SML. Similarly, Sabbaghzadeh et al. (2024) observed sporadic UV absorption shoulders across an Atlantic-wide survey, attributing them also to in situ MAAs production by phytoplankton and bacteria in high-UV environments. During both sampling events (01 July 2016 and 04 May 2017), surface slicks were clearly observed. Solar irradiance reached some of its annual maximum values (approximately 800 and 750 W m⁻², respectively), while consecutive Saharan dust episodes (30 and 40 μg m⁻³, of dust flux respectively) occurred concurrently. These conditions favoured intense phytoplankton activity as reflected by the elevated chlorophyll-a concentrations (0.88 and 0.58 μg L⁻¹, respectively) and corroborate to the release of MAAs into the consolidated SML, contributing to the UV absorption features observed in the CDOM spectra of Fig. 5. Although distinct spectral signatures of MAAs were not discernible during the remaining samplings, their occurrence provides clear evidence of biological processes within the SML that influence CDOM dynamics.

3.3. FDOM composition in the SML and ULW resolved by PARAFAC modelling

In Fig. 6 the components resolved by the PARAFAC model on SML and ULW EEMs are shown. Hereafter C1, C2, C3 and C4 will refer to the components and I_1 , I_2 , I_3 and I_4 to the intensities of the respective components in the SML and ULW samples.

386

387

388

389

390

391

392

393

394

395

396

397

398 399

400





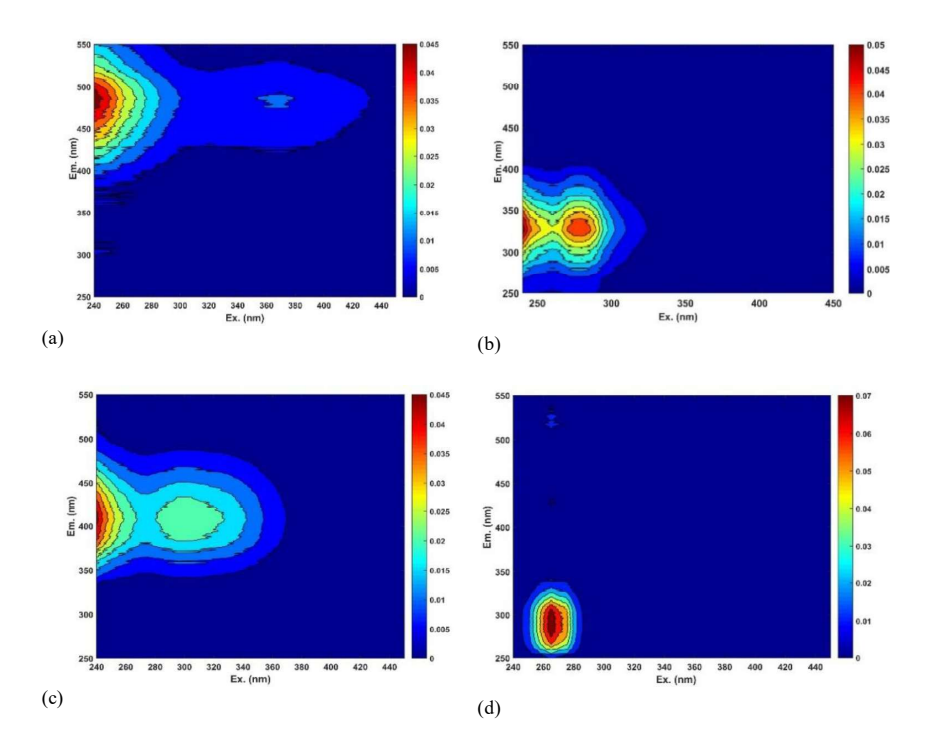


Figure 6: The four components resolved in the SML and ULW by the seawater PARAFAC model, (a) Component C1, peaks A/C, (b) Component C2, peak T, (c) Component C3, peaks A/M, (d) Component C4, peak B

Component C1 presented two excitation maxima at 240 nm and 375 nm and a single emission maximum at 486 nm that resembles peaks A and C described by Coble et al. (1990; 1998). Peak A (ex/em 240/486 nm) has been associated with aromatic highly conjugated humic material origin (McKnight et al., 2001), while peak C (ex/em 375/486 nm) reflects more mature, condensed aromatic humics also of terrestrial origin. The fact that peak C presents longer excitation wavelength compared to peak A implies that the organic substances that fluoresce in the region of peak C are of relatively higher molecular weight and aromaticity compared to the substances that fluoresce in the region of peak A (McKnight et al,2001). Component C2 presented excitation maxima at 240 nm and 280 nm and maximum at 338 nm and is associated with peak T (Coble et al., 1998). The spectral characteristics of component C2 indicate proteinaceous material that resembles tryptophan amino acid (Coble, 1996; Coble et al., 1998), indicative of autochthonous biological production in aquatic systems. The third component, C3 showed two excitation maxima at 240 nm and 295 nm and a single emission maximum at 408 nm. These two peaks resemble peaks A and M respectively. In this case peak A (ex/em 240/408 nm) is resolved in shorter wavelengths. Peak M (ex/em 295/408 nm) is indicative of lower molecular weight less aromatic humic substances predominately associated with in situ bacterial humification processes, while there are also references attributing to peak M terrestrial or riverine origin especially in estuaries and coastal





environments (Stedmon and Markager, 2005; Fellman et al., 2010; Catala et al., 2013). A common feature for PARAFAC modelling of FDOM in aquatic systems is that peak A may be deconvoluted in several components. This likely reflects the fact that the fluorescence associated with the humic-like peaks A, C, and M originates from aromatic chromophores that differ in their degree of conjugation, oxidation state, and source. Moreover, in coastal environments, dissolved organic matter is often enriched in lignin-derived compounds, originating from terrestrial plant material. Lignin exhibits strong UV absorption around 280 nm, which closely aligns with the excitation wavelength of fluorescence peak A, and fluoresces in the 420-470 nm range, overlapping with the emission regions of both fluorescence peaks A and C (Del Vecchio and Blough, 2004). Component C4 shows a single excitation and emission maximum at ex/em 270/290 nm similar to the maximum of peak B (Coble et al. 1998). Peak B is representative of proteinaceous material that resembles tyrosine amino acids. This organic material is associated to bacterial degradation processes in contrast to the proteinaceous peak T which is associated with primary production processes. All four components have been previously reported in the SML in the Mediterranean Sea and the global ocean (Galgani and Engel 2016; Pitta et al., 2017; Martinez-Perez et al., 2019; Drozdowska et al., 2018). In marine environments, humic-like fluorescent components are generally more susceptible to photodegradation than protein-like components. Several studies have shown that exposure to solar radiation leads to a marked decrease in the intensity of humic-like peaks (A, C, M), while the protein-like peaks (T, B) are comparatively less affected (Retelletti Brogi et al., 2020; Romera-Castillo et al., 2011; Zhang et al., 2013). Among the humic-like components, peak C typically exhibits the greatest sensitivity to photobleaching, followed by peak A (Helms et al., 2003; Retelletti Brogi et al., 2020).

3.4. FDOM dynamics within the CDOM pool in the SML and ULW

As illustrated from Y-axes in Fig. 7, in the SML during most months, components C1 (peak A–C) and C2 (peak T) exhibited higher intensities (I1: 0.033–0.398 R.U. and I2: 0.038–0.429 R.U.,) than components C3 (peak A–M) (I3: 0.016–1.249 R.U.) and C4 (peak B) (I4: 0–0.196 R.U.) consistent with their order of deconvolution by the PARAFAC model. Moreover, intensities show roughly equal contributions of the humic-like C1 and tryptophan-like C2 to the FDOM pool. Component C3 (peak A–M) had the highest average intensity (0.122 R.U.) and the widest range; however, this was largely due to an outlier recorded on 01 July 2016 (Fig. 7(c)). Excluding this outlier, C3 intensities remained considerably lower than those of C1 and C2. Component C4 (peak B) displayed the lowest values but higher variability (70.4%) with highest values during summer 2016 and lowest occurred from late winter (February) to mid-spring 2017 (Table S5). The two samplings on 01 July 2016 and 04 May 2017, which exhibited high DOC and a(λ) absorption values in the SML, also demonstrated exceptionally strong fluorescence intensities across all four PARAFAC components. In the ULW, components C1, C2, and C3 showed minimal variation overall, peaking during autumn bloom on 07 October 2016. In contrast, component C4 was more variable, with higher intensities from June to October 2016 (Table S5).





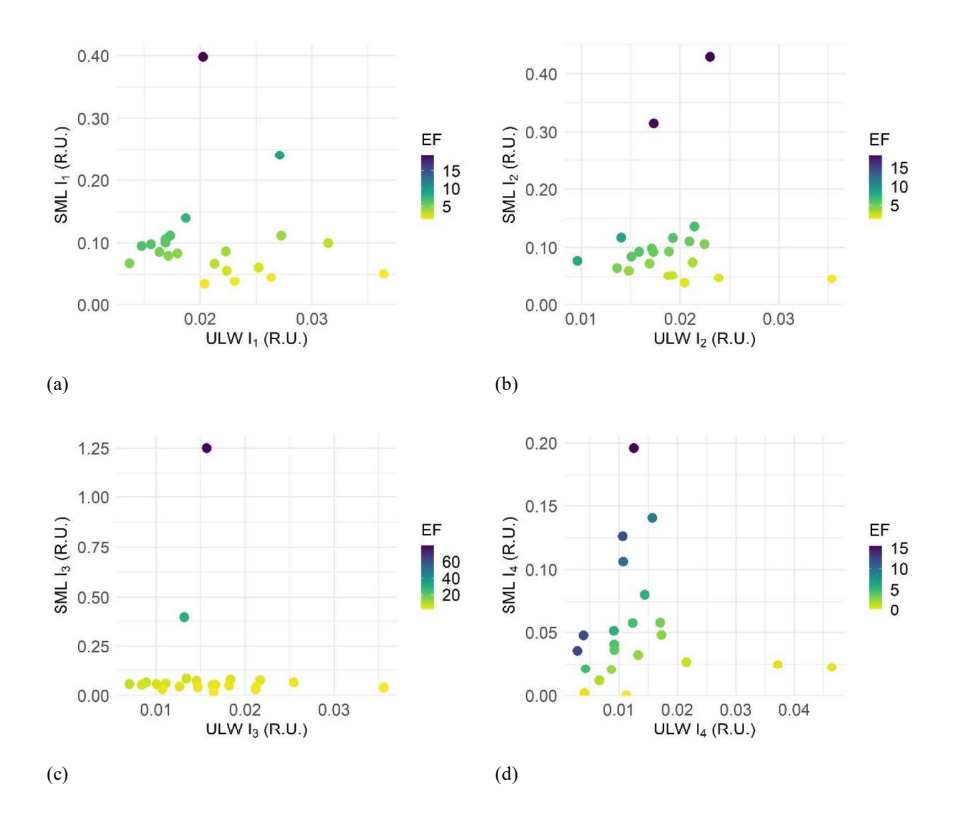


Figure 7: Correlation graphs between the SML (y axis) and ULW (x axis) of PARAFAC maximum fluorescence intensities (R.U.) of (a) I_1 ; (b) I_2 ; (c) I_3 ; (d) I_4 . The z axis illustrates the enrichment factors

The lack of correlation of the PARAFAC intensities $I_{1.4}$ between the SML and ULW (p>0.05), denotes a decoupling of processes acting upon FDOM in the two water layers (Fig. 7). As with DOC and CDOM, the SML is found enriched in FDOM with most of the EFs fluctuating well above 1 (p<0.05 in all cases) (Fig. 7, Table S4). In particular, the humic like fluorophores (peak A/C) and the tryptophan like one (peak T) appear the most enriched in the SML (average EF: 4.2 and 4.5 respectively). Yang et al. 2022, reported clearly higher EFs of the tryptophan-like peak in the SML compared the humic-like and tyrosine-like peaks, indicating a greater contribution of marine autochthonous DOM in the SML relative to the ULW. In our study, the FDOM enrichment within the SML appears to be more evenly distributed between humic (terrestrial) DOM and protein (autochthonous) DOM.

As described previously, PARAFAC modelling resolved the terrestrial humic-like fluorophores (peak A) into two components—C1 (peak A/C) and C2 (peak A/M)—reflecting overlapping emission regions

as described previously, PARAFAC modelling resolved the terrestrial numic-like fluorophores (peak A) into two components—C1 (peak A/C) and C2 (peak A/M)—reflecting overlapping emission regions typical of marine samples. However, this separation makes it difficult to directly assess the relationship between FDOM and CDOM compounds across the full spectral range. To investigate the relative contribution of FDOM to the bulk CDOM, we calculated the FDOM to CDOM index (FDOM/CDOM, R.U.·m) by dividing the full excitation–emission matrix (EEM) of each sample by the corresponding absorption coefficients at the respective excitation wavelengths, as described in Section 2.6 (Fig. S1). The average ratios for all SML and ULW samples are presented in the plots of Fig. 8. This approach

462

463

464

465

466

467

468

469

470

471

472

473

474

475

476

477

478

479

480





provides qualitative insight on the relative importance of the fluorescent to absorbing chromophores present in the two water layers.

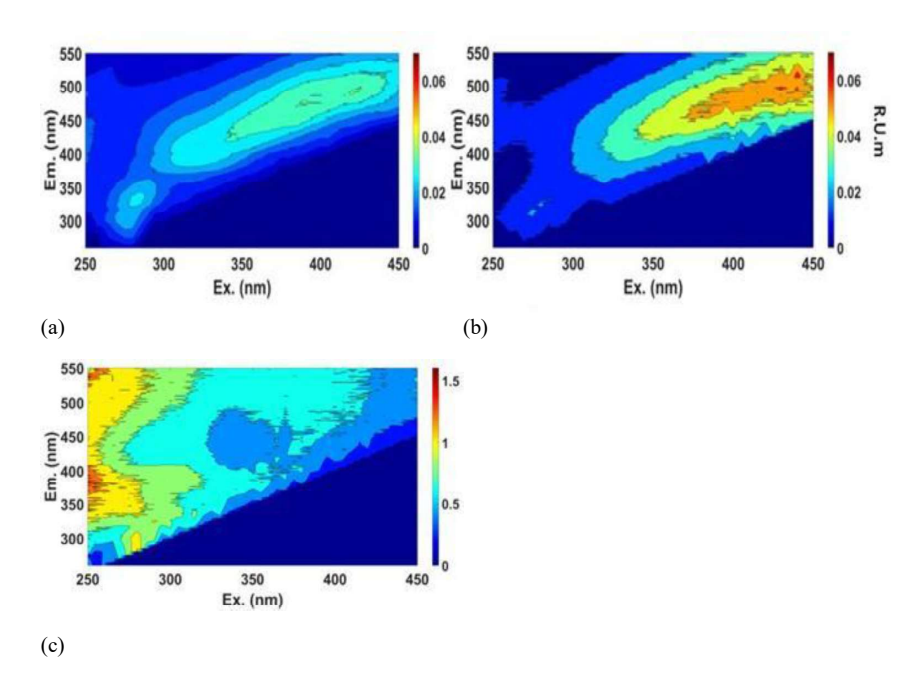


Figure 8: The FDOM/CDOM index (R.U.·m) in the (a) SML, (b) ULW, (c) the ratio (FDOM/CDOM)_{sml} / (FDOM/CDOM)_{ulw}. (a,b) Depletion of UV-a/near visible fluorescence is apparent in the SML relative to the ULW. (c) Higher contribution of short wavelength (UV-C/UV-B) FDOM to CDOM is apparent in the SML

Figure 8 (a, b) show that FDOM/CDOM index values are elevated at longer excitation wavelengths (>350 nm) relative to shorter wavelengths in both the SML and ULW, indicating a relatively higher contribution of UV-A/near-visible FDOM to bulk CDOM compared to UV-B and UV-C FDOM. Between layers, the SML appears less enriched in UV-A-near-visible FDOM compared to CDOM, likely reflecting the higher bulk CDOM content in the SML at these wavelengths, as discussed previously based on CDOM indices. CDOM enrichment factors (EFs) increased more than threefold from the UV-C to the UV-A region, consistent with selective enrichment of UV-A near visible chromophores. It appears that the humic-like FDOM fraction of CDOM is more susceptible to photodegradation than the corresponding humic CDOM fraction, and/or that humic CDOM is produced at a higher rate than humic FDOM within the SML. Photodegradation of terrigenous DOM, leads to the formation of lower molecular weight, less complex DOM with altered optical characteristics (Opsahl & Benner, 1998; Opsahl & Zepp, 2001; Obernosterer & Benner, 2004), while contrary plankton-derived DOM (mostly protein-like and low molecular weight substances) presents minimal photochemical alteration (Obernosterer and Benner, 2004). Previous studies have also demonstrated that FDOM exhibits stronger photodegradation at longer excitation wavelengths than at shorter ones (Helms et al., 2013; Gonsior et al., 2013). Particularly, Helms et al. (2013) observed that irradiation caused the emission maxima of humic-like peaks A and C to shift toward shorter wavelengths, with the greater shift occurring for peak C, while its excitation maximum





481 shifted toward longer wavelengths. At the same time, the SML may be influenced by atmospheric inputs 482 of water-soluble organic carbon (WSOC) with distinct optical signatures. For example, nitro-aromatic 483 compounds present in atmospheric WSOC exhibit strong absorption at 300-500 nm (Huang et al., 2021, 484 Lin et al., 2017) but show minimal fluorescence likely due to the significant reduction in the electron 485 density of the benzene ring by the nitro group (Chen et al., 2020, Cao et al. 2023). Because of the 486 hydrophobic nature of these aromatic compounds, they are expected to preferentially accumulate in the 487 SML. Overall, the various sources and complex DOM transformation processes occurring in the SML 488 appear to promote a more pronounced accumulation of absorbing but not fluorescent CDOM at longer 489 wavelengths. 490 In the UV-B and UV-C regions, where humic-like peak A and protein-like peaks T and B are observed 491 in the EEMs (Ex/Em = 250/485 nm), the FDOM/CDOM index is relatively low in both layers, suggesting 492 that highly absorbing material dominates over fluorescent material in this spectral range in both layers. 493 To examine differences between the SML and ULW in the low-wavelength region, we calculated the 494 ratio (FDOM/CDOM)_{sml} / (FDOM/CDOM)_{ulw} (Fig. 8(c)). This analysis revealed that the SML has a 495 relatively higher FDOM fraction at UV-C and UV-B wavelengths, indicating that the proportion of 496 highly aromatic, terrestrial humic material and freshly produced protein-like material is greater in the 497 SML than in the ULW. Terrestrial humics and lignin degradation products absorbing at the short UV-B 498 and UV-C regions can be small sized allochthonous molecules, resistant to photodegradation and are 499 expected to enter the coastal environments either via land runoff or via the atmosphere. (Hernes and 500 Benner, 2003; Jaffe et al., 2014) 501 The preferential enrichment of nitrogen organic compounds, mostly amino-acids, in the SML is 502 documented for diverse coastal and open waters (Liss and Duce, 1997; Kuznetsova and Lee, 2002; 503 Kuznetsova et al., 2004; van Pixteren et al., 2012; Cunliffe et al., 2013; Chen et al., 2022). It is 504 documented that amino acid enrichment in the SML is likely facilitated by other factors rather than excess 505 in situ production (Kuznetsova and Lee, 2002; Kuznetsova et al., 2004). Within the FDOM pool in 506 particular, the accumulation of amino acid like fluorophores (peaks T and B) has been attributed to 507 microbial release by photoprotection mechanisms and/or cell lysis (Galgani and Engel, 2016; Yang et 508 al., 2022). Our study provides indication of episodic MAAs production in the SML. Increased bacterial 509 production in the SML compared to the ULW has been reported in the Mediterranean Sea under the 510 influence of dry atmospheric deposition (Astrahan et al., 2016). As already stated, several dust events 511 occurred during the sampling period, likely stimulating bacterial activity and the subsequent production 512 of humic-like compounds in the SML. 513 Overall, the SML and ULW display distinct FDOM to CDOM profiles. The SML exhibits a higher 514 fluorescent fraction relative to bulk CDOM in the UV-C and UV-B regions (protein-like peaks and peak 515 A) but a lower fraction in the UV-A/near-visible range (peak C) compared to the ULW. Based on CDOM 516 and FDOM indices, the SML appears enriched in high molecular weight, non-fluorescent organic 517 compounds, together with low molecular weight fluorescent material of terrestrial and amino acid-like 518 origin. This pattern suggests that the SML acts as a selective accumulation layer, concentrating 519 photoreactive and surface-active DOM fractions, while bulk UV-A fluorescent material is comparatively





diluted, reflecting differential contributions of in situ production, atmospheric deposition, and selective
 photochemical or biological transformations.

Rain events are significant sources of dissolved organic carbon in surface seawater as it was estimated

522

3.4. Influence of Wet Deposition on SML Enrichment

523524525

526

527

528

529

530

531

532

533

534

535

536

537

538

539

540

541

542

543

544

545

546

547

548

549

550

551

552

553

554

555

556

557

558

559

that they contribute about 90 x 1012 g C yr⁻¹ (Willey et al., 2000). Rainwater can be exceptionally rich in CDOM (Kieber et al., 2006) while increased DOM concentrations in the SML during rain events have been reported (Wurl and Obbard 2005; Lim et al., 2007; Ribas-Ribas et al. 2017). Several sources contribute to water soluble organic carbon (WSOC) forms in the atmosphere, such as biomass burning, fossil fuel combustion, wind driven soil particulates, including Saharan dust, volatile organic compounds over urban areas, and sea spray over coastal and marine sites (Mladenov et al., 2011; Miyazaki et al., 2018). Studies on the optical properties of WSOC in the atmosphere have shown an overall similarity with the fluorophores found in the marine environment, i.e., humic-like and protein-like substances, yet with distinct differences in their spectral position (Wu et al., 2021 and references therein). Given the coastal location of the rainwater sampler near an urban area and the prevailing meteorological conditions, the collected samples are expected to reflect contributions from multiple sources. The objective of the CDOM/FDOM analysis in rainwater was to investigate potential linkages between the optical signatures of rainwater and those observed in the SML. DOC ranged from 0.60 to 6.26 mg L⁻¹ (average 2.49 mg L⁻¹). Absorption coefficients at 300 nm (a₃₀₀) varied between 0.931 and 8.070 m⁻¹ (average 3.395 m⁻¹), while the spectral slope S₂₇₅₋₂₉₅ exhibited a narrow range 0.021-0.030 nm⁻¹ (average 0.024 nm⁻¹) (Table S6). Rainwater DOM was highly enriched in optically active material, with a strong coupling observed between DOC and a(λ) (Table 1). Compared to the SML, rainwater exhibited comparable DOC concentrations, slightly higher a₃₀₀ values, and similar average spectral slope S275-295, though with a narrower range. PARAFAC analysis of the rainwater EEMs resolved three fluorescent components (R1, R2, and R3) (Table S6, Fig. 9). Component R1, with excitation maxima at 240 and 290 nm and an emission maximum at 394 nm, corresponds to peaks A and M and is analogous to seawater component C3, albeit slightly blue-shifted, suggesting a smaller molecular weight. This component was dominant with fluorescence intensities I₁ ranging from 0.108 R.U. to 1.09 R.U. Component R2 exhibited excitation maxima at 245 and 335 nm and an emission maximum at 456 nm, representing peaks A and C, and was similarly blue-shifted relative to seawater component C1. These spectral shifts indicate differences in the composition of aromatic, high-molecularweight humic substances between seawater and rainwater. Intensities of component R2 ranged from 0.025 R.U. to 0.389 R.U. Component R3, with excitation maxima at 240 and 270 nm and an emission maximum at 299 nm, corresponds to peak B, whose spectral characteristics closely match those observed in seawater. I₃ fluorescence intensities fluctuated in levels comparable to those of I₂, from 0.056 R.U. to 0.457 R.U., indicating an equal contribution of components R2 (peak A/C) and R3 (peak B) in rainwater FDOM. All identified rainwater components have been previously reported in studies of CDOM in precipitation (Müller et al., 2008; Santos et al., 2012; Yang et al., 2019). Notably, peak T, resolved in

seawater, was not resolved in the rainwater PARAFAC model.





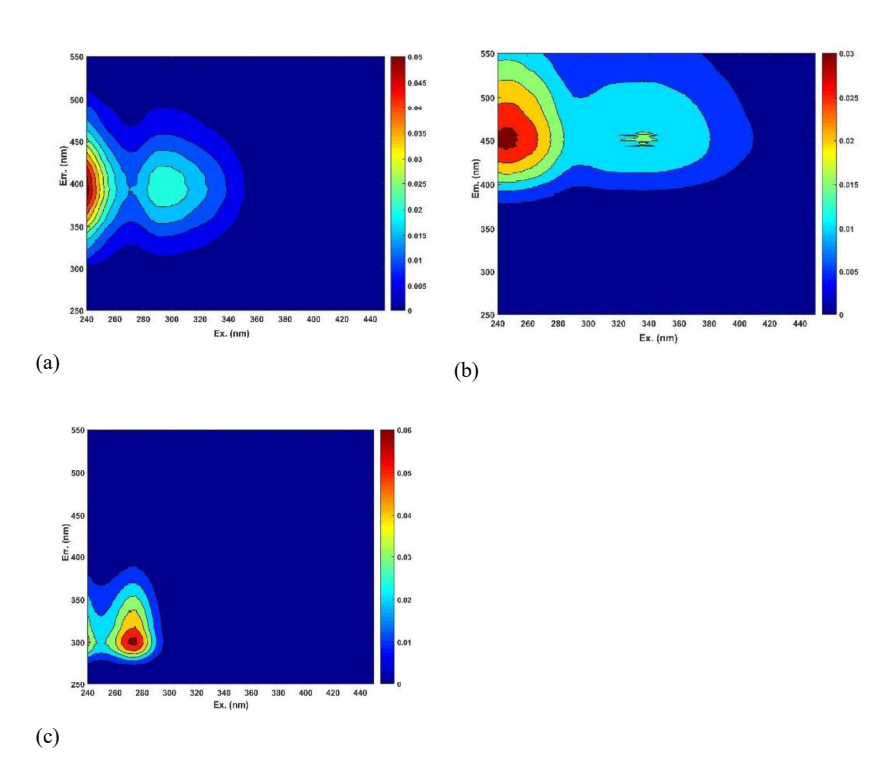


Figure 9: The three components resolved by the rainwater PARAFAC model, (a) Component R1, peaks A/M, (b) Component R2, peaks A/C, (c) Component R3, peak B

The predominance of humic-like fluorophores over protein-like ones in marine aerosols has been reported by Miyazaki et al. (2019), particularly within the spectral range of peak M fluorophores (Ex/Em = 300/400). These authors suggest that during the transfer of DOC to the atmosphere, protein-like compounds undergo substantial decomposition and/or there is preferential formation of humic-like substances in atmospheric aerosols. They also propose that the absence of protein-like fluorophores in sea spray may result from the strong association of these molecules with gel-like exopolymer colloids. Based on laboratory oxidation studies of atmospheric organic carbon, Fan et al. (2019) reported that various oxidation pathways—beyond simple photodegradation—affect atmospheric WSOC, including reactions with hydroxyl radicals (-OH), ozone (O₃), and nitrogen oxides (NO_x). In particular, tryptophan-like fluorophores were found to be highly susceptible to -OH oxidation, leading to their transformation into humic-like and tyrosine-like compounds. Moreover, several works on atmospheric humic-like substances provide evidence that during atmospheric transport degradation processes (photo- and oxidative ones) generate low molecular weight molecules, and of more aliphatic nature (Wu et al., 2021 and references therein).

Consistent with these findings, our data show a clear predominance of humic-like peaks A and M (component R1) in rainwater samples, the absence of tryptophan-like fluorophores among the





PARAFAC components, and blue shifted FDOM components R1 (peak A/M) and R2 (peak A/C). These features suggest: (i) a significant contribution of marine aerosols to rainwater over our study area, and (ii) effective photodegradation and oxidation processes leading to the depletion of tryptophan-like fluorophores and the formation of relatively low-molecular-weight, humic-like compounds. The optical signatures of the rainwater samples further indicate that wet deposition contributes to the CDOM/FDOM pool in the SML primarily through degraded, humic-like components of terrestrial origin (peaks A and C) and tyrosine-like amino acids. At the same time, the prevalence of marine humic-like fluorescence (peak M) points to an efficient recirculation of marine FDOM through sea spray derived marine aerosols. In parallel, the similarities in a_{300} and spectral slope values $S_{275-295}$ with the SML suggest that high molecular weight, light-absorbing but non-fluorescent compounds are present in both rainwater and the SML.

589 590

579

580

581

582

583

584

585

586

587 588

4. Conclusion

591592593

594

595

596

597

598

599

600

601

602

603

604

605

606

607

608

609

610

611

612

613

614

615

The SML exhibited consistent enrichment in DOM, CDOM and FDOM relative to the ULW. Upward transport from the ULW to the SML was found more important for bulk DOM while different processes seem to act upon the CDOM and FDOM pools within each layer. Although bulk CDOM was closely coupled to DOM in the SML, based on CDOM and FDOM indices we were able to discriminate variable accumulation patterns of the optically active organic material. Surprisingly the impact of photodegradation processes on the S275-295 vs a₃₀₀ relationship was less evident in the SML relatively to the ULW. This was attributed to the selective enrichment of high molecular weight optically active material in the UV-A/near visible region, as evidenced by the increase in $a(\lambda)$ EFs for longer wavelengths, and the lower S275-295 values relatively to the ULW. By introducing the FDOM/CDOM ratio we further revealed wavelength-dependent enrichment patterns: SML exhibited lower fraction of the more conjugated fluorophores at the UV-A/near visible range relatively to the ULW and higher fractions of low molecular weight terrestrial humics and protein like fluorophores in the UV-C, UV-B regions. In combination with CDOM indices, these observations suggest that the SML favors the selective accumulation of high molecular weight, non-fluorescent organic compounds alongside low molecular weight fluorescent material of terrestrial and amino-acid-like origin. Several parallel processes may contribute to these patterns including: i) biological transformation of DOM within the SML generating molecules of variable molecular weight, ii) fast reorganisation of the SML macromolecular structure, iii) atmospheric inputs of optically active DOM. For the latter our analysis in rainwater provided evidence of the presence of relatively low molecular weight fluorescent humic -like material (blue shifted peaks) while at the same time low spectral slopes point to the presence of non-fluorescent high molecular weight CDOM in wet deposition. In contrast, CDOM in the ULW exhibited weaker coupling with DOC, higher spectral slopes, and clear evidence of photodegradation, emphasizing the distinct processes governing DOM dynamics between the two layers.





617 specific DOM fractions accumulate relative to the underlying water, underscoring its chemical and biological significance in marine ecosystems. 618 619 620 **Data availability**: Detailed data are provided in the Supplementary material of this work. 621 622 Financial Support: This work has been supported by the National Monitoring Programme for the Implementation of WFD in Greece (MIS 5001676, Ministry for the Environment and Energy). 623 624 625 Author contribution: Writing (original draft preparation) EP, CZ; Investigation ET, EP; Formal Analysis EP, CZ; Writing (review and editing) EP, CZ, ET; Conceptualization CZ, ET, EP. 626 627 628 Acknowledgment: We wish to thank K. Fostiropoulos and T. Zoulias for the help in the fieldwork and 629 A. Konstantinopoulou for Chl-a analysis. English language has been revised using A.I. ChatGPT free 630 online tool 631 632 Competing interests: The authors declare that they have no conflict of interest. 633 634 References 635 Asher, W.: The sea-surface microlayer and its effect on global air-sea gas transfer, in: The sea surface 636 and global change, edited by: Liss, P.S., and Duce, R.A., Cambridge University Press, 251-286, https://doi.org/10.1017/CBO9780511525025.009, 1997 637 638 Astrahan, P., Herut, B., Paytan, A., Rahav, .: The Impact of Dry Atmospheric Deposition on the Sea-639 Surface Microlayer in the SE Mediterranean Sea: An Experimental Approach, Front. Mar. Sci., 3:222, 640 doi: 10.3389/fmars.2016.00222, 2016 641 Azimi, S., Ludwig, A., Thévenot, D.R., Colin, J-L.:Trace metal determination in total atmospheric 642 deposition in rural and urban areas, Sci. Total Environ., 308, 247-256, https://doi.org/10.1016/S0048-643 9697(02)00678-2, 2003 644 Cao, T., Li, M., Xu, C., Song, J., Fan, X., Li, J., Jia, W., and Peng, P.: Technical note: Chemical 645 composition and source identification of fluorescent components in atmospheric water-soluble brown 646 carbon by excitation-emission matrix spectroscopy with parallel factor analysis - potential limitations 647 and applications, Atmos. Chem. Phys., 23, 2613-2625, https://doi.org/10.5194/acp-23-2613-2023, 2023. 648 Catala, T.S., Mladenov, N., Echevarria, F., Reche, I.: Positive trends between salinity and chromophoric 649 and fluorescent dissolved organic matter in a seasonally inverse estuary, Estuar. Coast. Shelf Sci., 133, 650 206-216, http://dx.doi.org/10.1016/j.ecss.2013.08.030, 2013

Collectively, these findings highlight the SML as a dynamic, selectively enriched interface where





- 651 Chen, Y., Yang, G.P, Wu, G.W., Gao, X.C., Xia, Q.Y.: Concentration and characterization of dissolved
- organic matter in the surface microlayer and subsurface water of the Bohai Sea, Cont. Shelf Res., 52, 97
- 653 107, https://doi.org/10.1016/j.csr.2012.11.007, 2013
- 654 Chen, Y., Yang, G.P., Xia, Q.Y., Wu, G.W.: Enrichment and characterization of dissolved organic matter
- 655 in the surface microlayer and subsurface water of the South Yellow Sea, Mar. Chem., 182, 1-13,
- 656 https://doi.org/10.1016/j.marchem.2016.04.001, 2016
- 657 Chen, Q., Li, J., Hua, X., Jiang, X., Mu, Z., Wang, M., Wang, J., Shan, M., Yang, X., Fan, X., Song, J.,
- 658 Wang, Y., Guan, D., and Du, L.: Identification of species and sources of atmospheric chromophores by
- 659 fluorescence excitation-emission matrix with parallel factor analysis, Sci. Total Environ., 718, 137322,
- 660 https://doi.org/10.1016/j.scitotenv.2020.137322, 2020.
- 661 Chen, Y., Zhang, N., Hu, C., Chen, R., and Yang, G.-P.: Controls on the distribution, enrichment, and
- degradation of dissolved organic matter in the sea surface microlayer of the Yellow Sea and East China
- 663 Sea, J. Geophys. Res. Oceans, 127, https://doi.org/10.1029/2022JC019122, 2022
- 664 Chin, Y. P., G. Aiken, OLoughlin, E.,: Molecular-weight, polydispersity, and spectroscopic properties
- 665 of aquatic humic substances, Environ. Sci. Technol., 28, 1853–1858, doi: 10.1021/es00060a015, 1994
- 666 Coble, P. G., Green, S. A., Blough, N. V., and Gagosian, R. B.: Characterisation of dissolved organic
- matter in the Black Sea by fluorescence spectroscopy, Nature, 348, 432-435, doi: 10.1038/348432a0,
- 668 1990.
- 669 Coble, P. G.: Characterization of marine and terrestrial DOM in seawater using excitation emis5699 sion
- 670 matrix spectroscopy, Mar. Chem., 51, 325–346, doi: 10.1016/0304-4203(95)00062-3, 1996.
- 671 Coble, P. G., Del Castillo, C. E., and Avril, B.: Distribution and optical properties of CDOM in the
- Arabian Sea during the 1995 southwest monsoon, Deep-Sea Res. Pt. II, 45, 2195-2223,
- 673 https://doi.org/10.1016/S0967-0645(98)00068-X, 1998.
- 674 Coble, P. G.: Marine optical biogeochemistry: the chemistry of ocean color, Chem. Rev., 107, 402–418,
- 675 https://doi.org/10.1021/cr050350+, 2007
- 676 Cunliffe, M., Salter, M., Mann, P.J., Whiteley, A.S., Upstill-Goddard, R.C., Murrell, J.C.: Dissolved
- 677 organic carbon and bacterial populations in the gelatinous surface microlayer of a Norwegian fjord
- 678 mesocosm, FEMS Microbiol. Lett., 299, 248–254, https://doi.org/10.1111/j.1574-6968.2009.01751.x,
- 679 2009
- 680 Cunliffe, M., Engel, A., Frka, S., Gašparović, B., Guitart, C., Murrell, J.C., Salter, M., Stolle, C., Upstill-
- 681 Goddard, R., Wurl, O.: Sea surface microlayers: A unified physicochemical and biological perspective
- 682 of the air—ocean interface, Prog. Oceanogr., 109, 104–116, https://doi.org/10.1016/j.pocean.2012.08.004,
- 683 2013





- 684 Del Vecchio, R., Blough, N.V.: On the origin of the optical properties of humic substances. Environ. Sci.
- 685 Technol., 38, 3885-3891, doi: 10.1021/es049912h, 2004
- 686 Drozdowska, V., Kowalczuk, P., Konik, M., Dzierzbicka-Glowacka, L.: Study on Different Fractions of
- 687 Organic Molecules in the Baltic Sea Surface Microlayer by Spectrophoto- and Spectrofluorimetric
- 688 Methods, Front. Mar. Sci. 5, 456,
- 689 Ebling, A. and Landing, W.M.: Trace elements in the sea surface microlayer: rapid responses to changes
- 690 in aerosol deposition, Elementa: Sci. Anthropocene, 5:42, https://doi.org/10.1525/elementa.237, 2017
- 691 Engel, A. and Galgani, L.: The organic sea-surface microlayer in the upwelling region off the coast of
- 692 Peru and potential implications for air-sea exchange processes, Biogeosciences, 13, 989-1007,
- 693 https://doi.org/10.5194/bg-13-989-2016, 2016.
- 694 Fan, X., Yu, X., Wang, Y., Xiao, X., Li, F., Xie, Y., Wei, S., Song, J., Peng, P.: The aging behaviors of
- 695 chromophoric biomass burning brown carbon during dark aqueous hydroxyl radical oxidation processes
- 696 in laboratory studies, Atmos. Environ., 213, 391–400, doi:10.1016/j.atmosenv.2019.116909, 2019
- 697 Fellman, J.B., Hood, E., Spencer, R.G.M.: Fluorescence spectroscopy opens new windows into dissolved
- 698 organic matter dynamics in freshwater ecosystems: A review, Limnol., Oceanogr., 55, 2452-2462,
- 699 https://doi.org/10.4319/lo.2010.55.6.2452, 2010.
- 700 Fichot, C.G. and Benner, R.: A novel method to estimate DOC cocentrations from CDOM absorption
- 701 coefficients in coastal waters, Geophy. Res. Lett., 38, doi:10.1029/2010GL046152, 2011.
- 702 Gallisai, R., Peters, F., Volpe, G., Basart, S., Baldasano, J.M.: Saharan Dust Deposition May Affect
- 703 Phytoplankton Growth in the Mediterranean Sea at Ecological Time Scales, PLoS ONE, 9,
- 704 doi:10.1371/journal.pone.0110762, 2014
- 705 Gao, H., Zepp, R. G.: Factors influencing photoreactions of dissolved organic matter in a coastal river of
- 706 the Southeastern United States, Environ. Sci. Technol., 32, 2940 2946,
- 707 https://doi.org/10.1021/es9803660, 1998
- 708 Gonsior, M., Schmitt-Kopplin, P., Bastviken, D.: Depth-dependent molecular composition and photo-
- 709 reactivity of dissolved organic matter in a boreal lake under winter and summer conditions,
- 710 Biogeosciences, 10, 6945–6956, doi:10.5194/bg-10-6945-2013, 2013
- 711 Hardy, J.T.: The sea surface microlayer: Biology, chemistry and anthropogenic enrichment, Prog.
- 712 Oceanogr., 11, 307-328, https://doi.org/10.1016/0079-6611(82)90001-5, 1982
- 713 Harvey, G.W. and Burzell, L.A.: A Simple Microlayer Method for Small Samples, Limnol. Oceanogr.,
- 714 11, 608-614. doi:10.4319/lo.1966.11.4.0608, 1972
- 715 Helms, J.R., Stubbins, A., Ritchie, J.D., Minor, E.C., Kieber, D.J., Mopper, K.: Absorption spectral
- 716 slopes and slope ratios as indicators of molecular weight, source, and photobleaching of chromophoric





- 717 dissolved organic matter, Limnol. Oceanogr., 53, 955-969, https://doi.org/10.4319/lo.2008.53.3.0955,
- 718 2008
- 719 Helms, J. R., Stubbins, A., Perdue, E. M., Green, N. W., Chen, H., Mopper, K.: Photochemical bleaching
- 720 of oceanic dissolved organic matter and its effect on absorption spectral slope and fluorescence, Mar.
- 721 Chem., 155, 81–91, doi:10.1016/j.marchem.2013.05.015, 2013
- 722 Hernes, P. J., and Benner, R.: Photochemical and microbial degradation of dissolved lignin phenols:
- 723 Implications for the fate of terrigenous dissolved organic matter in marine environments, J. Geophys.
- 724 Res. Oceans, 108(C9), 3291, doi:10.1029/2002JC001421, 2003

- 726 Hoge, F.E., Williams, M.E., Swift, R.N., Yungel, J.K., Vodacek, A.: Satellite retrieval of the
- 727 absorptioncoefficient of chromophoric dissolved organic matter in continental marginal, J. Geophys.
- 728 Res., 100, https://doi.org/10.1029/95JC02561, 24847–24854, 1995

- 730 Huang, R.-J., Yang, L., Shen, J., Yuan, W., Gong, Y., Ni, H., Duan, J., Yan, J., Huang, H., You, Q., and
- 731 Li, Y. J.: Chromophoric Fingerprinting of Brown Carbon from Residential Biomass Burning, Environ.
- 732 Sci. Technol. Let., 9, 102–111, https://doi.org/10.1021/acs.estlett.1c00837, 2021.
- 733 Hunter, K.A.: Processes affecting particulate trace metals in the sea surface microlayer, Mar. Chem., 9,
- 734 49–70, https://doi.org/10.1016/0304-4203(80)90006-7, 1980
- 735 Jaffé, R., Cawley, K. M., and Yamashita, Y.: Applications of Excitation Emission Matrix Fluorescence
- 736 with Parallel Factor Analysis (EEM-PARAFAC) in Assessing Environmental Dynamics of Natural
- 737 Dissolved Organic Matter (DOM) in Aquatic Environments: A Review, ACS Symp. Ser., 1160, 27-
- 73, doi:10.1021/bk-2014-1160.ch003, 2014
- 739 Kieber, R. J., Whitehead, R. F., Reid, S. N., Willey, J. D., and Seaton, P. J.: Chromophoric dissolved
- 740 organic matter (CDOM) in rainwater, Southeastern North Carolina, USA, J. Atmos. Chem., 54, 21–41,
- 741 doi:10.1007/s10874-005-9008-4, 2006
- 742 Kirk, J. T. O.: Light and Phytosynthesis in Aquatic Ecosystems, 2nd ed., Cambridge Univ. Press, New
- 743 York., 509 pp, ISBN 9780511623370, 1994
- 744 Kitsiou, D., Karydis, M.: Categorical mapping of marine eutrophication based on ecological indices, Sci
- 745 Total Environ, 255, 113-27, doi: 10.1016/s0048-9697(00)00457-5, 2000
- 746 Kuznetsova, M. and Lee, C.: Dissolved free and combined amino acids in nearshore seawater, sea surface
- 747 microlayers and foams: influence of extracellular hydrolysis, Aquat. Sci., 64, 252-268,
- 748 https://doi.org/10.1007/s00027-002-8070-0, 2002
- 749 Kuznetsova, M., Lee, C., Aller, J., Frew, N.: Enrichment of amino acids in the sea surface microlayer at
- 750 coastal and open ocean sites in the North Atlantic Ocean, Limnol. Oceanogr., 49, 1605-1619,
- 751 https://doi.org/10.4319/lo.2004.49.5.1605, 2004





- 752 Lawaetz, A.J., Stedmon, C.A.: Fluorescence intensity calibration using the Raman scatter peak of water,
- 753 Appl Spectrosc, 63, 936-940. doi: 10.1366/000370209788964548, 2009
- 754 Lechtenfeld, O. J., Kattner, G., Flerus, R., McCallister, S. L., Schmitt-Kopplin, P., Koch, B. P., Molecular
- 755 transformation and degradation of refractory dissolved organic matter in the Atlantic and Southern
- 756 Ocean, Geochim. Cosmochim. Acta, 126, 321-337. https://doi.org/10.1016/j.gca.2013.11.009, 2014
- 757 Lim, L., Wurl, O., Karuppiah, S., and Obbard, J. P.: Atmospheric wet deposition of PAHs to the
- 758 sea-surface microlayer, Mar. Pollut. Bull., 54(8), 1212–1219, doi:10.1016/j.marpolbul.2007.03.023,
- 759 2007
- 760 Lin, P., Bluvshtein, N., Rudich, Y., Nizkorodov, S. A., Laskin, J., and Laskin, A.: Molecular Chemistry
- 761 of Atmospheric Brown Carbon Inferred from a Nationwide Biomass Burning Event, Environ. Sci.
- 762 Technol., 51, 11561–11570, https://doi.org/10.1021/acs.est.7b02276, 2017.
- 763 Liss, P.S. and Duce, R.A. (Eds.): The sea surface and global change. Cambridge University Press, 519
- 764 pp., ISBN 9780511525025,
- 765 https://doi.org/10.1017/CBO9780511525025, 1997
- 766 Logozzo, L., Tzortziou, M., Neale, P., Clark, B J.: Photochemical andmicrobial degradation of
- 767 chromophoricdissolved organic matter exportedfrom tidal marshes, J. Geophys. Res.: Biogeosciences,
- 768 126, https://doi.org/10.1029/2020JG005744, 2021
- 769 Martínez-Pérez, A. M., Catalá, T. S., Nieto-Cid, M., Otero, J., Álvarez, M., Emelianov, M., Reche, I.,
- 770 Álvarez-Salgado, X. A., and Arístegui, J.: Dissolved organic matter (DOM) in the open Mediterranean
- 771 Sea. II: Basin-wide distribution and drivers of fluorescent DOM, Prog. Oceanogr., 170, 93-106,
- 772 doi:10.1016/j.pocean.2018.10.019, 2019
- 773 McKnight, D., M., Boyer, E.W., Westerhoff, P.K., Doran, P.T., Thomas Kulbe, T., Andersen, D.T.:
- 774 Spectrofluorometric characterization of dissolved organic matter for indication of precursor organic
- 775 material and aromaticity, Limnol. Oceanogr., 46, 38-48, https://doi.org/10.4319/lo.2001.46.1.0038, 2001
- 776 Milinković, A., Penezić, A., Kušan, A.C., Gluščić, V., Žužul, S., Skejić, S., Šantić, D., Godec, R.,
- 777 Pehnec, G., Omanović, D., 712 Engel, A., Frka, S.: Variabilities of biochemical properties of the sea
- 778 surface microlayer: Insights to the atmospheric deposition impacts, Sci. Total Environ., 838, 156440,
- 779 https://doi.org/10.1016/j.scitotenv.2022.156440, 2022
- 780 Miyazaki, Y., Yamashita, Y., Kawana, K., Tachibana, E., Kagami, S., Mochida, M., Suzuki, K.,
- 781 Nishioka, J.: Chemical transfer of dissolved organic matter from surface seawater to sea-spray
- water-soluble organic aerosol in the marine atmosphere, Sci. Rep., 8, 14861, doi:10.1038/s41598-018-
- 783 32864-7, 2018
- 784 Mladenov, N., Sommaruga, R., Morales-Baquero, R., Laurion, I., Camarero, L., Diéguez, M.C.,
- 785 Camacho, A., Delgado, A., Torres, O., Chen, Z., Felip, M., and Reche, I.: Dust inputs and bacteria





- 786 influence dissolved organic matter in clear alpine lakes, Nat. Commun., 2, 405,
- 787 doi:10.1038/ncomms1411, 2011
- 788 Mopper, K., Zhou, X., Kieber, R. J., Kieber, D.J., Sikorski, R. J., Jones, R.D.: Photochemical degradation
- 789 of dissolved organic carbon and its impact in the oceanic carbon cycle, Nature, 353, 60-62,
- 790 https://doi.org/10.1038/353060a0, 1991
- 791 Moran, M.A., Sheldeon, W.M., Zepp, R.G.: Carbon loss and optical property changes during long term
- 792 photochemical and biological degradation of estuarine dissolved organic matter. Limnol. Oceanogr., 45,
- 793 1254–1264, https://doi.org/10.4319/lo.2000.45.6.1254, 2000
- 794 Muller, C. L., Baker, A., Hutchinson, R., Fairchild, I. J., Kidd, C.: Analysis of rainwater dissolved
- 795 organic carbon compounds using fluorescence spectrophotometry. Atmospheric Environment, 42, 8036-
- 796 8045. https://doi.org/10.1016/j.atmosenv.2008.06.042, 2008
- 797 Murphy, K., Stedmon, C.A., Graeber, D., Bro, R., Fluorescence spectroscopy and multi-way techniques.
- 798 PARAFAC, Anal. Methods, 5, doi: 10.1039/c3ay41160e, 2013
- 799 Mustaffa, N.I.H., Ribas-Ribas M., Wurl O.: High-resolution variability of the enrichment of fluorescence
- 800 dissolved organic carbon in the sea surface microlayer of an upwelling region, Elementa-Sci. Anthrop.,
- 801 5:242, https://doi.org/10.1525/elementa.242, 2017
- 802 Mustaffa, N.I.H., Badewien, T.H., Ribas-Ribas, M, Wurl, O.: High-resolution observations on
- enrichment processes in the sea-surface microlayer, Sci. Rep., 8, 13122, https://doi.org/10.1038/s41598-
- 804 018-31465-8, 2018
- 805 Mustaffa, N.I.H., Ribas-Ribas, M., Banko-Kubis, H.M., Wurl, O.: Global reduction of in situ CO₂
- transfer velocity by natural surfactants in the sea-surface microlayer, Proc. R. Soc. Math. Phys. Eng. Sci.,
- 807 476, 20190763, https://doi.org/10.1098/rspa.2019.0763, 2020
- 808 Nelson, N.B., Siegel, D.A., Michaels, A.,F.: Seasonal dynamics of colored dissolved material in the
- 809 Sargasso Sea, Deep Sea Res., Part I, 45, 931–957, https://doi.org/10.1016/S0967-0637(97)00106-4, 1998
- 810 Nelson, N.B. and Siegel, D.A.: The global distribution and dynamics of chromophoric dissolved organic
- 811 matter, Ann. Rev. Mar. Sci., 5, 447-476, doi: 10.1146/annurev-marine-120710-100751, 2013
- 812 Obernosterer, I., and Benner, R.: Competition between biological and photochemical processes in the
- 813 mineralisation of dissolved organic carbon, Limnol. Oceanogr., 49, 117-124,
- 814 doi:10.4319/lo.2004.49.1.0117, 2004
- Obernosterer, I., Catala, P., Lami, R., Caparros, J., Ras, J., Bricaud, A., Dupuy, C., van Wambeke, F.,
- 816 Lebaron, P.: Biochemical characteristics and bacterial community structure of the sea surface microlayer
- 817 in the South Pacific Ocean, Biogeosciences, 5, 693-705, https://doi.org/10.5194/bg-5-693-2008, 2008





- 818 Opsahl, S., and Benner, R.: Photochemical reactivity of dissolved lignin in river and ocean waters,
- 819 Limnol. Oceanogr., 43, 1297–1304, doi:10.4319/lo.1998.43.6.1297, 1998
- 820 Opsahl, S. P., and Zepp, R. G.: Photochemically-induced alteration of stable carbon isotope ratios (δ^{13} C)
- 821 in terrigenous dissolved organic carbon, Geophys. Res. Lett., 28, 2417-2420,
- 822 doi:10.1029/2000GL012686, 2001
- 823 Ortega-Retuerta, E., Frazer, T.K., Duarte, C.M., Ruiz-Halpern, S., Tovar-Sanchez, A., Arrieta, J.M.,
- 824 Reche, I.: Biogeneration of chromophoric dissolved organic matter by bacteria and krill in the Southern
- 825 Ocean, Limnol. Oceanogr., 54, 1941-1950, 2009
- 826 Osmund, H.H. and Riemann, B., Chlorophyll a Determination: Improvements in Methodology, Oikos,
- 827 30, 438–447, https://doi.org/10.2307/3543338, 1978
- 828 Penezić, A., Drozdowska, V., Novak, Gašparović, B.: Distribution and characterization of organic matter
- 829 within the sea surface microlayer in the Gulf of Gdańsk, Oceanologia, 4, 631-650,
- 830 https://doi.org/10.1016/j.oceano.2022.05.003, 2022
- 831 Pitta, E., Zeri, C., Tzortziou, M., Mousdis, G., Scoullos, M.: Seasonal variations in dissolved organic
- 832 matter composition using absorbance and fluorescence spectroscopy in the Dardanelles Straits North
- 833 Aegean Sea mixing zone, Cont. Shelf Res., 149, 82-95, https://doi.org/10.1016/j.csr.2016.07.013, 2017
- 834 Pitta, E., & Zeri, C.: The impact of combining data sets of fluorescence excitation-emission matrices of
- 835 dissolved organic matter from various aquatic sources on the information retrieved by PARAFAC
- modelling, Spectrochim. Acta A Mol. Biomol. Spectrosc., 258, 119800, 2021.
- 837 Pereira, R., Ashton, I., Sabbaghzadeh, B., Shutler, J.D., Upstill-Goddard, R.C.: Reduced air-sea CO2
- 838 exchange in the Atlantic Ocean due to biological surfactants, Nat. Geosci., 11, 492-496,
- 839 https://doi.org/10.1038/s41561-018-0136-2, 2018
- 840 Ploug, H.: Cyanobacterial surface blooms formed by Aphanizomenon sp. and Nodularia spumigena in
- the Baltic Sea: small-scale fluxes, pH, and oxygen microenvironments, Limnol. Oceanogr., 53, 914–921,
- 842 https://doi.org/10.4319/lo.2008.53.3.0914, 2008
- 843 Retelletti Brogi, S., Charrière, B., Gonnelli, M., Vaultier, F., Sempéré, R., Vestri, S., Santinelli, C.: Effect
- 844 of UV and Visible Radiation on Optical Properties of Chromophoric Dissolved Organic Matter Released
- 845 by Emiliania huxleyi, J. Mar. Sci. Eng., 8(11), 888, doi:10.3390/jmse8110888, 2020
- 846 Ribas-Ribas, M., Mustaffa, N.I.H., Rahlff, J., Stolle, C. and Wurl, O.: Sea Surface Scanner (S3): A
- 847 catamaran for high-resolution measuremnets of biochemical properties of the sea surface microlayer, J.
- 848 Atmos. Oceanic. Technol., 34, 1433–1448, https://doi. org/10.1175/JTECH-D-17-0017.1, 2017
- 849 Romera-Castillo, C., Nieto-Cis, M., Castro, C.G., Marrase, C., Largier, J., Barton, E.D., Alvarez-
- 850 Salgado, X.A.: Fluorescence: absorption coefficient ratio tracing photochemical and microbial





- 851 degradation processes affecting coloured dissolved organic matter in a coastal system, Mar. Chem., 125,
- 852 26-38, https://doi.org/10.1016/j.marchem.2011.02.001, 2011.
- 853 Sabbaghzadeh, B., Upstill-Goddard, R.C., Beale, R. Pereira, R. Nightingale, P.D.: The Atlantic Ocean
- 854 surface microlayer from 50°N to 50°S is ubiquitously enriched in surfactants at wind speed up to 13 m s
- 855 ¹, Geophys. Res. Lett,. 44, 2852-2858, https://doi.org/10.1002/2017GL072988, 2017
- 856 Sabbaghzadeh, B., Uher, G., Upstill-Goddard, R.: Dynamics of chromophoric dissolved organic matter
- 857 in the Atlantic Ocean: unravelling province-dependent relationships, optical complexity, and
- 858 environmental influences, Front. Mar. Sci., 11, https://doi.org/10.3389/fmars.2024.1432133, 2024
- 859 Santos, P. S. M., Santos, E. B. H., Duarte, A. C.: First spectroscopic study on the structural features of
- 860 dissolved organic matter isolated from rainwater in different seasons, Sci. Total Environ., 426, 172–179,
- 861 doi:10.1016/j.scitotenv.2012.03.023, 2012
- 862 Siegel, D. A., and Michaels, A.F.: Quantification of non-algal light attenuation in the Sargasso Sea:
- 863 Implications for biogeochemistry and remote sensing, Deep Sea Res., Part II, 43, 321-345,
- 864 https://doi.org/10.1016/0967-0645(96)00088-4, 1996
- 865 Stedmon C.A. and Markager, S.: Tracing the production and degradation of autochthonous fractions of
- 866 dissolved organic matter by fluorescence analysis, Limnol. Oceanogr., 50, 1415-1426,
- 867 https://doi.org/10.4319/lo.2005.50.5.1415, 2005
- 868 Stolle, C., Nagel, K., Labrenz, M., Jurgens, K.: Succession of the sea-surface microlayer in the coastal
- 869 Baltic Sea under natural and experimentally induced low-wind conditions, Biogeosciences, 7, 2975-
- 870 2988, https://doi.org/10.5194/bg-7-2975-2010, 2010
- 871 Tassan, S.: The effect of dissolved yellow substance on the quantitative retrieval of chlorophyll and total
- 872 suspended sediment concentration from remote measurements of water colour, Int. J. Remote Sens., 9,
- 873 787–797, https://doi.org/10.1080/01431168808954893, 1988
- 874 Tilstone, G.H., Airs, R.L., Vicente, V.M., Widdicombe, C., Llewellyn, C., High concentrations of
- 875 mycosporine-like amino acids and colored dissolved organic matter in the sea surface microlayer off the
- 876 Iberian Peninsula, Limnol. Oceanogr. 55, 1835–1850. doi: 10.4319/lo.2010.55.5.1835, 2010
- 877 Twardowski, M.S. and Donaghay, P.L.: Separating in situ and terrigenous sources of absorption by
- 878 dissolved materials in coastal waters, J. Geophys. Res., 106, 2545-2560,
- https://doi.org/10.1029/1999JC000039, 2001
- 880 Tzempelikou, E., Zeri, C., Pitta, E., Assimakopoulou, G., Pavlidou, A., Rousselaki, E.: Temporal
- 881 dynamics of transparent exopolymer particles in surface waters and sea surface microlayer in the coastal
- 882 Eastern Mediterranean Sea, Reg. Stud. Mar. Sci, 85, https://doi.org/10.1016/j.rsma.2025.104163, 2025





- 883 Tzortziou, M., Neale, P.J., Megonigal, J.P., Pow, C.L., Butterworth, M., Spatial gradients in dissolved
- 884 carbon due to tidal marsh outwelling into a Chesapeake Bay estuary, Mar. Ecol. Prog. Ser., 426, 41–56,
- 885 doi: 10.3354/meps09017, 2011
- 886 Upstill-Goddard, R.C.: Air-sea gas exchange in the coastal zone, Estuar. Coast. Shelf Sci., 70, 388-404,
- 887 https://doi.org/10.1016/j.ecss.2006.05.043, 2006
- 888 van Pinxteren, M., Mav E., Herrmann, H., Herrmann, H.: Chemical characterization of dissolved organic
- 889 compounds from coastal sea surface microlayers (Baltic Sea, Germany), Environ. Sci. Technol., 46,
- 890 10455–10462, doi:10.1021/es204492b, 2012.
- 891 Weishaar, J.L., Aiken, G.R., Bergamaschi, B.A., Fram, M.S., Fujii, R., Mopper, K.: Evaluation of
- 892 Specific Ultraviolet Absorbance as an Indicator of the Chemical Composition and Reactivity of
- 893 Dissolved Organic Carbon, Environ. Sci. Technol., 37, 4702–4708, https://doi.org/10.1021/es030360x,
- 894 2003
- 895 Willey, J.D., Kieber, R.J., Eyman, M.S., Avery, G.B.Jr.: Rainwater dissolved organic carbon:
- 896 concentrations and global flux, Glob. Biogeochem. Cycles, 14(1), 139–
- 897 148, doi:10.1029/1999 GB900036, 2000
- 898 Wu, G., Fu, P., Ram, K., Song, J., Chen, Q., Kawamura, K., Wan, X., Kang, S., Wang, X., Laskin, A.,
- 899 Cong, Z.: Fluorescence characteristics of water-soluble organic carbon in atmospheric aerosol,
- 900 Environ. Pollut., 268, 115906, doi:10.1016/j.envpol.2020.115906, 2021
- 901 Wurl, O. and Obbard, J.P.: A review of pollutants in the sea-surface microlayer (SML): a unique habitat
- 902 for marine organisms, Mar. Pollut. Bull., 48, 1016-1030,
- 903 https://doi.org/10.1016/j.marpolbul.2004.03.016, 2004
- 904 Wurl, O. and Holmes, M.: The gelatinous nature of the sea-surface microlayer, Mar. Chem., 110, 89-97,
- 905 https://doi.org/10.1016/j.marchem.2008.02.009, 2008
- 906 Wurl, O., Miller, L., Röttgers, R., Vagle, S.: The distribution and fate of surface-active substances in the
- 907 sea-surface microlayer and water column, Mar. Chem., 115, 1-9,
- 908 https://doi.org/10.1016/j.marchem.2009.04.007, 2009
- 909 Wurl, O., Stolle, C., Van Thuoc, C., The Thu, P., Mari, X.: Biofilm-like properties of the sea surface and
- 910 predicted effects on air-sea CO2 exchang, Prog. Oceanogr. doi: 10.1016/j.pocean.2016.03.002, 2016
- 911 Yang, L., Chen, W., Zhuang, W.-E., Cheng, Q., Li, W., Wang, H., Guo, W., Chen-Tung Arthur Chen,
- 912 Liu, M.: Characterization and bioavailability of rainwater dissolved organic matter at the southeast coast
- 913 of China using absorption spectroscopy and fluorescence EEM-PARAFAC, Mar. Chem., 210, 11-22,
- 914 doi:10.1016/j.marchem.2018.10.021, 2019





- Yang, L., Zhang, J., Engel, A., Yang, G.-P.: Spatio-temporal distribution, photoreactivity and
 environmental control of dissolved organic matter in the sea-surface microlayer of the eastern marginal
- 917 seas of China, Biogeosciences, 19, 5251–5268, doi:10.5194/bg-19-5251-2022, 2022
- 918 Zäncker, B., Bracher, A., Röttgers, R., Engel, A., Variations of the Organic Matter Composition in the
- 919 Sea Surface Microlayer: A Comparison between Open Ocean, Coastal, and Upwelling Sites Off the
- 920 Peruvian Coast, Front. Microbiol., 8:2369, doi: 10.3389/fmicb.2017.02369, 2017
- 921 Zepp, R.G., Callaghan, T.V., Erickson, D.J.: Effects of en-hanced solar ultraviolet radiation on
- 922 biogeochemical cycles, J. Photochem. Photobiol., B Biol., 46, 69 82, https://doi.org/10.1016/S1011-
- 923 1344(98)00186-9, 1998
- 924 Zervoudaki, S., Siokou, I., Krasakopoulou, E., Kontoyiannis, H., Pavlidou, A., Assimakopoulou, G.,
- 925 Katsiaras, N., Reizopoulou, S., Karageorgis, A.P., Kaberi, H., Lardi, P.I., Gerakaris, V., Tsiamis, K.,
- 926 Salomidi, M., Zeri, C., Pitta, E., Strogyloudi, E., Parinos, C., Hatzianestis, I., Christou, E.D., Zoulias, T.,
- 927 Sakavara, A., Pagou, K., Zenetos, A., Panayotidis, P., Simboura, N.: Biogeochemical Characteristics in
- 928 the Saronikos Gulf (Aegean Sea, Eastern Mediterranean), in: The Aegean Sea Environment:
- 929 Anthropogenic Presence and Impact, edited by Anagnostou, C.L., Kostianoy, A.G., Mariolakos, I.D.,
- 930 Panayotidis, P., Soilemezidou, M., Tsaltas G., Hdb Environ. Chem., Springer, 142, 511-568,
- 931 https://doi.org/10.1007/698 2022 898, 2022
- 932 Zhang, Z., Cai, W., Liu, L., Liu, C., Chen, F.: Direct determination of thickness of sea surface microlayer
- 933 using a pH microelectrode at original location, Sc. China Ser. B-Chem, 46, 339-351,
- 934 https://doi.org/10.1360/02yb0192, 2003
- 935 Zhang, X. Y., Chen, X., Deng, H., Du, Y., Jin, H. Y.: Absorption features of chromophoric dissolved
- 936 organic matter (CDOM) and tracing implication for dissolved organic carbon (DOC) in Changjiang
- 937 Estuary, China, Biogeosciences Discuss., 10, 12217-12250, https://doi.org/10.5194/bgd-10-12217-
- 938 2013, 2013.
- P39 Zhang, Y., Liu, X., Osburn, C.L., Wang, M., Qin, B., Zhou, Y.: Photobleaching response of different
- 940 sources of chromophoric dissolved organic matter exposed to natural solar radiation using absorption
- 941 and excitation-emission matrix spectra, PLoS One, 8(10):e77515. doi: 10.1371/journal.pone.0077515,
- 942 2013

944

945

946